GeoStorage

Vol. 2, No. 2, p. 172-179, 2026

Research article

Experimental Study on Gas–Water Relative Permeability Behavior during Multi-Cycle Injection–Production in Gas Reservoir Storage

Kaijie Wang[1,2], Haijun Mao[2,3]*, Xiaojun Dai[1]

[1] *School of Civil Engineering and Geomatics, Southwest Petroleum University, Chengdu 610500, China*
[2] *Institute of Rock and Soil Mechanics, Chinese Academy of Sciences, Wuhan 430071,China*
[3] *State Key Laboratory of Geomechanics and Engineering Safety, Wuhan 430071, China*

Keywords:
Depleted gas reservoir
underground gas storage
multi-cycle injection–production
relative permeability
hysteresis effect

Cited as:
Wang KJ, Mao HJ, Dai XJ. 2026. Experimental Study on Gas–Water Relative Permeability Behavior during Multi-Cycle Injection–Production in Gas Reservoir Storage. *GeoStorage*, 2(2), 172-179. https://doi.org/10.46690/gs.2026.02.05

Abstract:
Converting depleted gas reservoirs into underground gas storage (UGS) is a critical strategic measure for ensuring national energy security and meeting peak-shaving and supply demands. During long-term multi-cycle injection–production operations, the rock pore structure and fluid distribution within the reservoir undergo dynamic evolution, leading to marked changes in gas–water relative permeability characteristics, which in turn directly affect the evaluation of effective working gas capacity and the design of pressure-boosting and capacity-expansion schemes. In this study, typical core samples were collected from a depleted-gas-reservoir UGS facility in Xinjiang. Multi-cycle gas–water alternating displacement experiments were performed using the unsteady-state method under high-temperature and high-pressure conditions (95 °C, 40–45 MPa), while triaxial cyclic loading–unloading was applied to simulate in-situ stress perturbations. The results reveal that with increasing injection–production cycles, the gas phase becomes trapped as isolated bubbles under the influence of the strong water-wettability of the rock and interfacial tension, causing the residual gas saturation to rise significantly (average increase of approximately 12%–15%). The gas-phase relative permeability curve shifts downward as a whole, exhibiting a pronounced cyclic hysteresis phenomenon. Concurrently, the irreducible water saturation gradually decreases, and the isotonic point of the two phases moves toward the lower left. A comparison of different operating pressure conditions shows that after boosting the pressure to 45 MPa, although the total gas-filled pore volume increases slightly owing to the reduction of irreducible water, the residual gas trapping effect intensifies, and the effective working gas capacity faces a risk of decline. This study elucidates the evolution mechanisms of gas–water flow capacity under multi-cycle injection–production and provides a crucial theoretical foundation and data support for the dynamic evaluation of storage capacity and the engineering practice of pressure boosting and capacity expansion.

1 Introduction

Natural gas, as a clean and efficient fossil fuel, plays an irreplaceable role during the energy transition. Underground gas storage (UGS) serves as a “regulator” and “stabilizer” in the natural gas production, supply, storage, and marketing system, and its peak-shaving and supply-security capability is directly linked to national energy security. UGS facilities converted from depleted oil and gas reservoirs have become the dominant type worldwide and in China owing to their well-characterized geological conditions, existing infrastructure, and low construction costs (Wei et al., 2026; Hu et al., 2024; He et al., 2026). However, unlike newly developed gas reservoirs, a depleted gas reservoir repurposed for injection–production operations un-

Yandy Scientific Press

* Corresponding author.
E-mail address: 1650735052@qq.com (Wang KJ); hjmao@whrsm.ac.cn (Mao HJ); neildai@swpu.edu.cn (Dai XJ)

Received Apr. 6, 2026; revised Apr. 16, 2026; accepted Apr. 24, 2026; available online May. 18, 2026.

dergoes a complex succession of processes—from water-drive gas/oil recovery to gas-drive water displacement and eventually to multi-cycle alternating gas–water displacement.

Over the full life-cycle of UGS operation, frequent cyclic injection–production loads not only induce periodic fluctuations in formation pressure but also cause irreversible damage to or restructuring of the microscopic pore structure of the reservoir, thereby altering gas–water two-phase flow characteristics. In particular, relative permeability—a key parameter—is not constant but exhibits dynamic evolution influenced by wettability changes, stress sensitivity, and fluid saturation history (Foroudi et al., 2022; Amri et al., 2024; Carlson, 1981; Land, 1968; Killough, 1976; Spiteri et al., 2008). Current UGS capacity evaluation methods are mostly based on static geological models or single-cycle displacement experiments, often neglecting the relative permeability hysteresis effect and the progressive accumulation of residual gas saturation induced by multiple injection–production cycles (Gao et al., 2023; Wang et al., 2024; Song et al., 2024; Gao et al., 2025; Fatemi , 2015). Furthermore, "pressure boosting and capacity expansion" has become an important technical approach to further unlock the potential of aging UGS facilities (Yang et al., 2023; Gao et al., 2022). Raising the maximum operating pressure alters the in-situ stress state and fluid occurrence environment, yet the mechanisms by which this influences gas–water flow behavior under multi-cycle injection–production remain unclear (Wei et al., 2026).

Based on the engineering background of a depleted-gas-reservoir UGS in Xinjiang, representative core samples were selected, and a high-temperature, high-pressure physical simulation experimental platform for multi-cycle injection–production was established (Thabit and Stephen, 2025; Johnson et al., 1959; Jones et al., 1978; Mehdi et al., 1986). Multi-cycle gas–water alternating displacement experiments were designed under different confining pressures (40 MPa and 45 MPa) to systematically analyze the effects of injection–production cycles, stress perturbations, and operating pressure on the shape of gas–water relative permeability curves, characteristic saturations, and flow capacity (Wang et al., 2024; Jello et al., 2022; Yang et al., 2024; Deng et al., 2023; Wang et al., 2025; Mi et al, 2018).

2 Experimental procedure

2.1 Sample selection and preparation

The experimental cores were obtained from Well X of a UGS in Xinjiang, from the sampling interval of 3289–3778 m, with a coring depth of 4091.8 m. The reservoir lithology in this block is predominantly sandstone, exhibiting typical low-to-medium porosity and low-to-medium permeability characteristics. In accordance with the Standard for Test Methods of Engineering Rock Mass (GB/T 50266-99), the field-retrieved cores were machined into standard cylindrical specimens with a diameter of 2.50 cm (tolerance ±0.03 cm) and a length of 5.00 cm (tolerance ±0.05 cm), with strict control of end-face parallelism and perpendicularity. Through basic petrophysical property measurements (porosity and permeability) on multiple candidate cores, four representative cores were selected for the experiments, covering two typical reservoir types: "medium porosity and medium permeability" and "low porosity and low permeability". The specific petrophysical parameters are presented in Table 1. Cores 1 and 2 represent the medium-to-high permeability zone, while Cores 3 and 4 represent the low permeability zone, thereby adequately reflecting the influence of reservoir heterogeneity on flow behavior.

2.2 Experimental apparatus and conditions

The experiment employed a high-temperature, high-pressure multi-functional core flooding system, as shown in Fig. 1. The main components are as follows:

1. Core holder: capable of applying a confining pressure of up to 60 MPa to simulate the overburden formation pressure and variations in pore pressure.

2. Fluid injection system: a high-precision dual-cylinder constant-rate/constant-pressure pump, used for injecting synthetic formation water (CaCl_2 type) and the experimental gas (high-purity nitrogen/methane).

3. Measurement and control system: comprising high-sensitivity pressure transducers (accuracy 0.1% FS), a back-pressure valve, and a gas mass flow meter, enabling real-time monitoring of the inlet–outlet differential pressure, flow rate, and temperature.

4. Data acquisition system: automatically records parameters such as pressure, flow rate, and temperature, with an adjustable sampling frequency.

The experimental conditions were set to closely match the actual field conditions of the target underground gas storage:

Temperature: constantly controlled at 95°C (the original reservoir temperature).

Pressure system: two upper pressure limits were established—the original design pressure of 40 MPa and the post-boosting pressure of 45 MPa to investigate the influence of pressure boosting and capacity expansion on relative permeability.

Fluid properties: synthetic CaCl_2 formation water was prepared with a salinity identical to that of the field water; high-purity nitrogen was selected to replace natural gas for the displacement experiments, considering both safety and the similarity in physical properties.

2.3 Experimental procedure and design

The gas–water relative permeability was measured using the unsteady-state method (modified JBN method). The detailed procedure is as follows:

1. Core pretreatment: The core samples were cleaned to remove residual oil, dried, weighed, and the air permeability and pore volume were determined.

2. Vacuum saturation: The samples were evacuated to below 133 Pa and saturated with synthetic formation water for more than 48 hours, after which the initial water saturation was calculated.

3. Establishment of irreducible water state: Under constant temperature and confining pressure, gas was injected to displace water from the core until no water was produced at the outlet and the gas production rate stabilized (displacement exceeding 20 PV). The volume of produced water was recorded, and the irreducible water saturation, S_{wc}, and the gas permeability at irreducible water saturation were calculated.

Tab. 1 Experimental core data

Core No.	Diameter (cm)	Length (cm)	Porosity (%)	Permeability (mD)
Core 1	2.52	5.00	15.29	22.75
Core 2	2.51	4.97	13.92	26.09
Core 3	2.49	5.02	10.58	1.10
Core 4	2.50	5.03	10.92	2.10

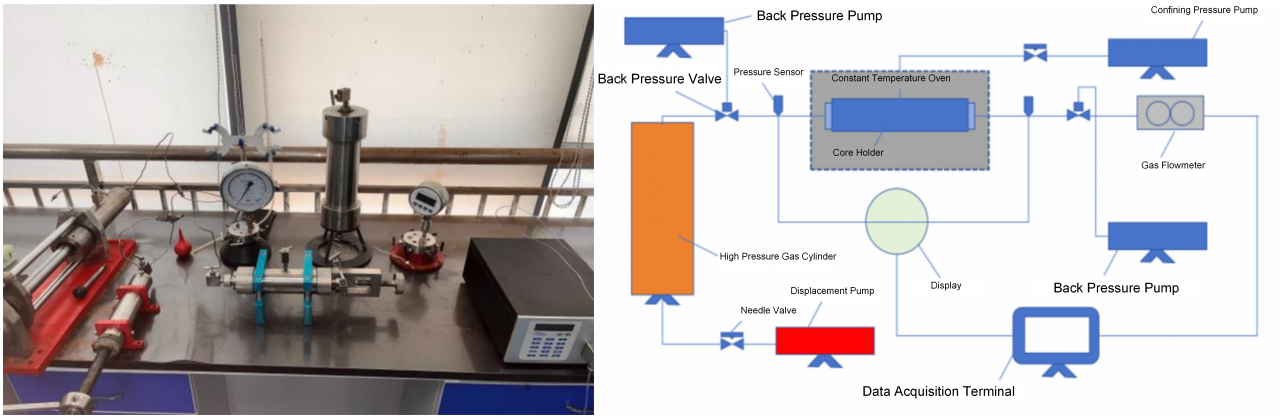

Fig. 1 Relative permeability measurement apparatus

4. Multi-cycle alternating displacement: First cycle (simulation of initial UGS construction): A complete water-displacing-gas process was performed, with pressure and production data recorded until the residual gas saturation state was reached.

Stress perturbation simulation: Between the first and second cycles, triaxial cyclic loading–unloading tests (axial pressure cycling between 15–40/45 MPa) were conducted on the cores to simulate the modification of the pore structure caused by formation stress fluctuations during injection–production operations.

Second cycle (simulation of multi-cycle operation): After re-saturating with water, another gas-displacing-water followed by water-displacing-gas cycle was carried out to simulate the second injection–production cycle.

5. Data processing: Based on the real-time monitored pressure differences and cumulative production, the gas and water relative permeabilities, K_{rg} and K_{rw}, were calculated at different saturations.

A total of four experimental schemes were designed (see Tab.2), corresponding to different permeability levels and operating pressure conditions. Two cycles of testing were completed for each scheme to compare the cyclic variations.

3 Experimental results

3.1 Saturation evolution

After two cycles of gas–water alternating displacement, the characteristic saturation parameters of the four cores changed significantly. Tab.3 summarizes the irreducible water saturation (Swc), residual gas saturation (Sgr), and recovery efficiency for each core from the two cycles.

The data show that for all cores, the irreducible water saturation decreased and the residual gas saturation increased significantly in the second cycle. In particular, the low-permeability cores (Cores 3 and 4) exhibited a substantial increase in residual gas saturation. For Core 3, the value surged from 4.63% to 35.19%, indicating that low-permeability reservoirs are more prone to gas phase trapping during multi-cycle operations. Concurrently, some cores (e.g., Cores 1 and 2) showed a slight increase in pore volume after the second cycle.

3.2 Changes in relative permeability curve morphology

Figs. 2–5 present the comparison of gas–water relative permeability curves for each core from the two experimental cycles.

For the medium-permeability cores (Cores 1 and 2):

Water phase: The water relative permeability (Krw) curve in the second cycle is overall slightly higher than or close to that of the first cycle, with flow capacity improvement particularly evident in the low-to-medium water saturation range. This may be associated with improved pore connectivity resulting from multi-cycle flushing.

Gas phase: The gas relative permeability (K_{rg}) curve in the second cycle shifts markedly downward. At the same water saturation, the gas flow capacity declines. For Core 1, for example, at a water saturation of 20%, the second-cycle Krg decreased by approximately 15% compared with the first cycle.

The relative permeability curves of the low-permeability cores exhibit greater dispersion between the two cycles. For Core 3, the second-cycle Krw curve drops extremely rapidly, approaching zero at a water saturation of 55%, whereas the first-cycle Krw still maintains a value of 0.30.

Gas breakthrough occurs earlier but with a limited peak: In the second cycle, gas permeability initiates at a lower water saturation (i.e., earlier gas breakthrough), but the overall peak

Tab. 2 Experimental design parameters

Experimental Group No.	Core Sample	Confining Pressure (MPa)	Temperature (°C)	Saturation Water Type	Test Method	Confining Pressure (MPa)	Axial pressure (MPa)
1	Core 1	40	95	$CaCl_2$	Unsteady-state	40	15–40
2	Core 2	45	95	$CaCl_2$	Unsteady-state	45	15–40
3	Core 3	40	95	$CaCl_2$	Unsteady-state	40	15–45
4	Core 4	45	95	$CaCl_2$	Unsteady-state	45	15–45

Tab. 3 Experimental results of relative permeability

Core No.	Experimental cycle	Dry weight (g)	Wet weight (g)	Pore volume (cm^3)	Porosity (%)	Irreducible water saturation (%)	Residual gas saturation (%)	Recovery (%)
Core 1	Cycle 1	56.06	59.87	3.81	15.29	8.14	25.20	72.57
Core 1	Cycle 2	56.15	60.08	3.93	15.77	5.09	37.15	60.86
Core 2	Cycle 1	53.79	57.12	3.33	13.92	12.61	21.62	75.26
Core 2	Cycle 2	54.19	57.78	3.59	15.00	13.65	32.03	62.90
Core 3	Cycle 1	59.32	61.91	2.59	10.58	45.95	4.63	91.43
Core 3	Cycle 2	59.58	61.74	2.16	8.82	21.30	35.19	55.29
Core 4	Cycle 1	58.46	61.15	2.69	10.92	42.38	3.72	93.55
Core 4	Cycle 2	58.77	61.12	2.35	9.54	28.51	14.89	79.17

value does not increase significantly and declines rapidly during the high-recovery stage. This indicates that although gas breaks through more easily, the number of effective flow channels does not increase; instead, the later-stage flow is impeded due to substantial bubble trapping.

3.3 Effect of pressure boosting and capacity expansion on relative permeability: a comparison

Under the pressure-boosted condition of 45 MPa, the irreducible water saturation of the cores was generally lower than that under the 40 MPa condition, indicating that elevated pressure helps overcome capillary resistance and expel more irreducible water from micropores, thereby increasing the theoretical gas-filled pore volume. However, the higher pressure simultaneously intensifies gas dissolution and diffusion effects, which, combined with stress sensitivity, results in a higher absolute value of residual gas saturation in the second cycle. This implies that although pressure boosting and capacity expansion increase the "total storage capacity", they may sacrifice a portion of the "effective recoverable reserves."

4 Results and discussion

4.1 Mechanism of relative permeability hysteresis under multi-cycle injection–production

The experimental results clearly reveal the relative permeability hysteresis effect during multi-cycle injection–production in depleted-gas-reservoir UGS. The core mechanisms are as follows:

(1) Jamin effect and gas bubble trapping: The reservoir rock is generally strongly water-wet. During the water-displacing-gas stage (gas withdrawal period), edge and bottom water invades gas-filled pores. Owing to capillary forces, the continuous gas phase is segmented into isolated bubbles (ganglia) and trapped in pore throats or dead ends. As injection–production cycles increase, this "snap-off and trapping" process recurs, causing residual gas saturation to accumulate cycle by cycle. The trapped gas occupies effective flow channels but cannot participate in flow, directly resulting in an overall downward shift of the gas relative permeability curve.

(2) Stress sensitivity of the pore structure: Pressure fluctuations during injection–production (simulated by triaxial cyclic loading–unloading) induce elastic/plastic deformation of the rock skeleton. For low-permeability tight sandstones, stress loading may cause closure of some micropores, while the hysteresis effect during unloading may generate new microcracks or enlarge existing throats. The observed changes in pore volume and relative permeability curve morphology confirm the remodeling effect of stress perturbations on the microscopic flow field.

(3) Dynamic evolution of wettability: Prolonged gas–water interaction may alter the wettability of the rock surface (change in contact angle), thereby affecting the capillary pressure curve. Although this study focuses primarily on macroscopic relative permeability, slight shifts in wettability are sufficient to cause movement of the isotonic point (a shift toward the lower left was observed in the experiments).

4.2 Implications for UGS capacity evaluation

Traditional storage capacity evaluation often assumes that relative permeability curves are constant or only considers single-cycle displacement characteristics. This study shows that such assumptions lead to significant deviations in UGS subjected to multi-cycle operations. With increasing years of

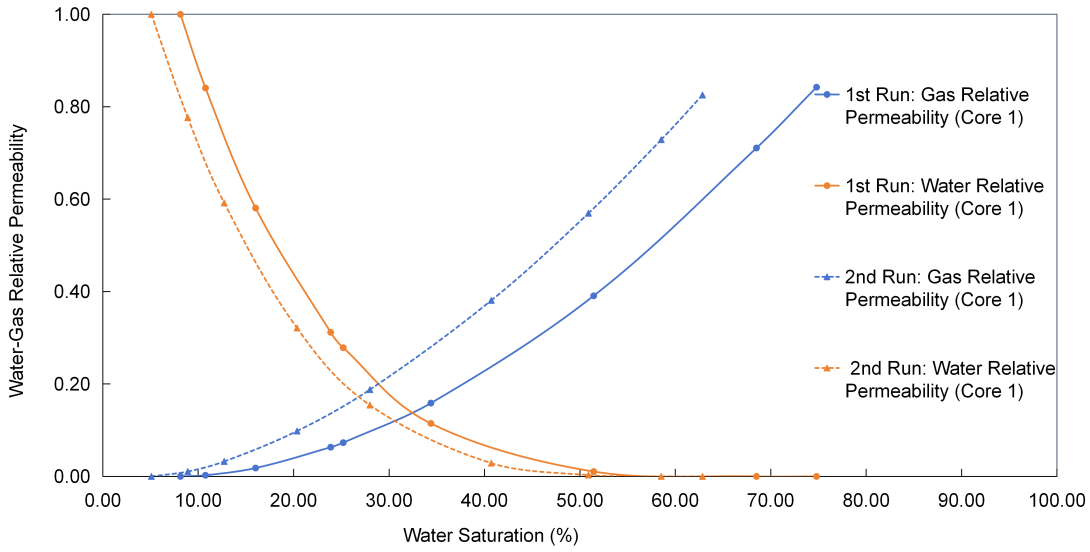

Fig. 2 Water–gas relative permeability curves (experimental group 1)

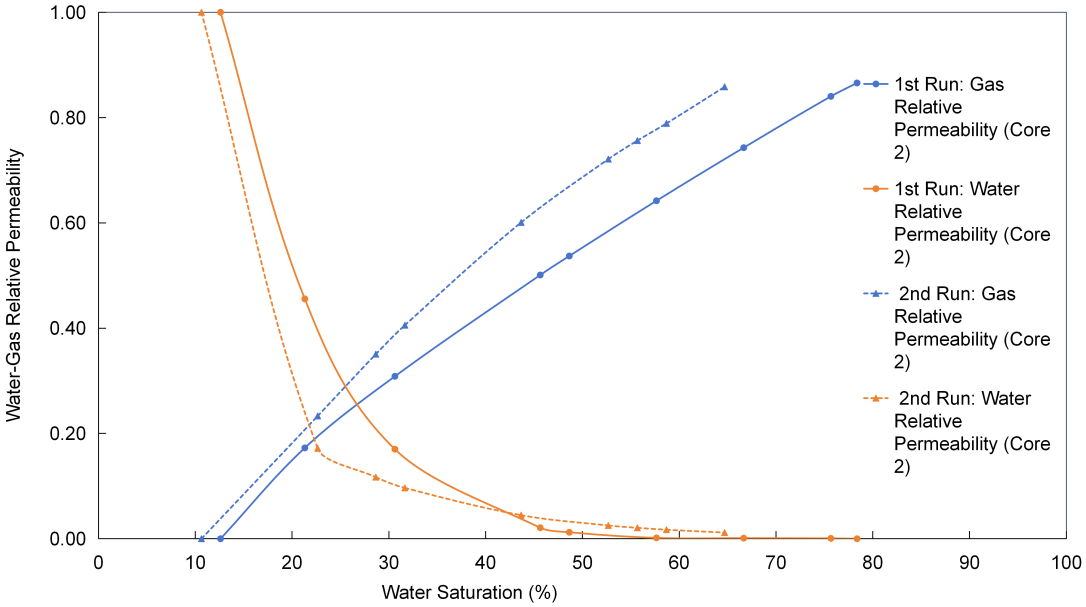

Fig. 3 Water–gas relative permeability curves (experimental group 2)

operation, the continuous rise in residual gas saturation means that an increasing proportion of pore space is occupied by "dead gas" and the recoverable fraction of effective working gas (recovery efficiency) exhibits a declining trend. Experimental data indicate that the recovery efficiency in the second cycle decreased by 10%–15% on average compared with the first cycle.

The double-edged sword effect of pressure boosting and capacity expansion: Although pressure-boosting operation (45 MPa) increases the total gas-bearing space by reducing irreducible water saturation, which is beneficial for enhancing total storage capacity, it simultaneously intensifies the gas trapping effect, leading to a decrease in the proportion of effectively recoverable reserves. Therefore, when formulating pressure-boosting schemes, one cannot rely solely on the increase in geological storage capacity; rather, the multi-cycle relative permeability evolution pattern must be incorporated to dynamically calculate the effective working gas volume, thus avoiding blind pressure boosting that may reduce peak-shaving efficiency.

4.3 Specific challenges for low-permeability reservoirs

A comparison between medium-permeability and low-permeability cores reveals that low-permeability reservoirs

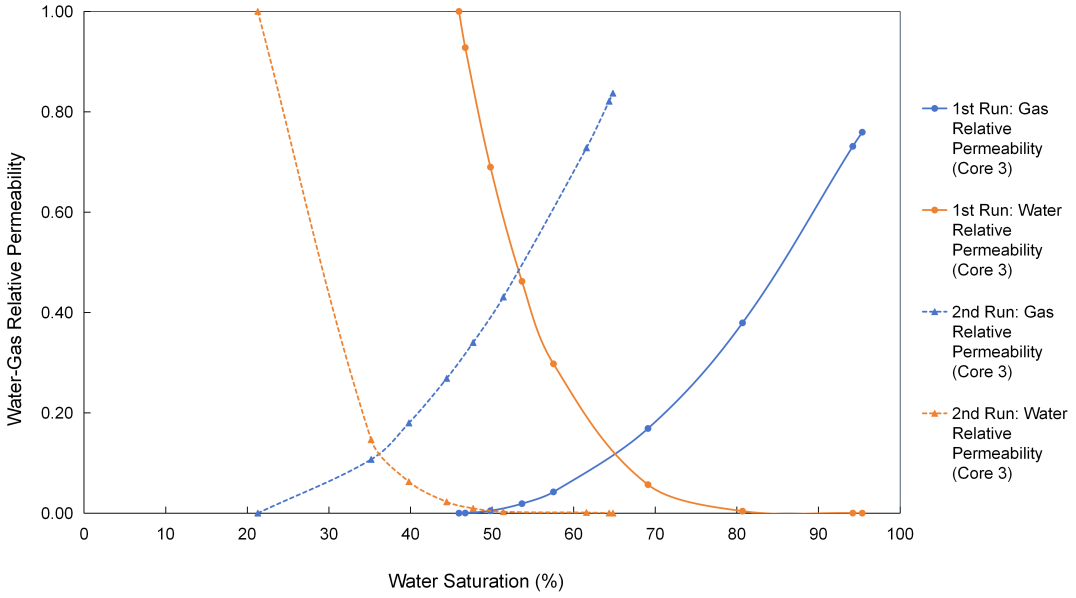

Fig. 4 Water–gas relative permeability curves (experimental group 3)

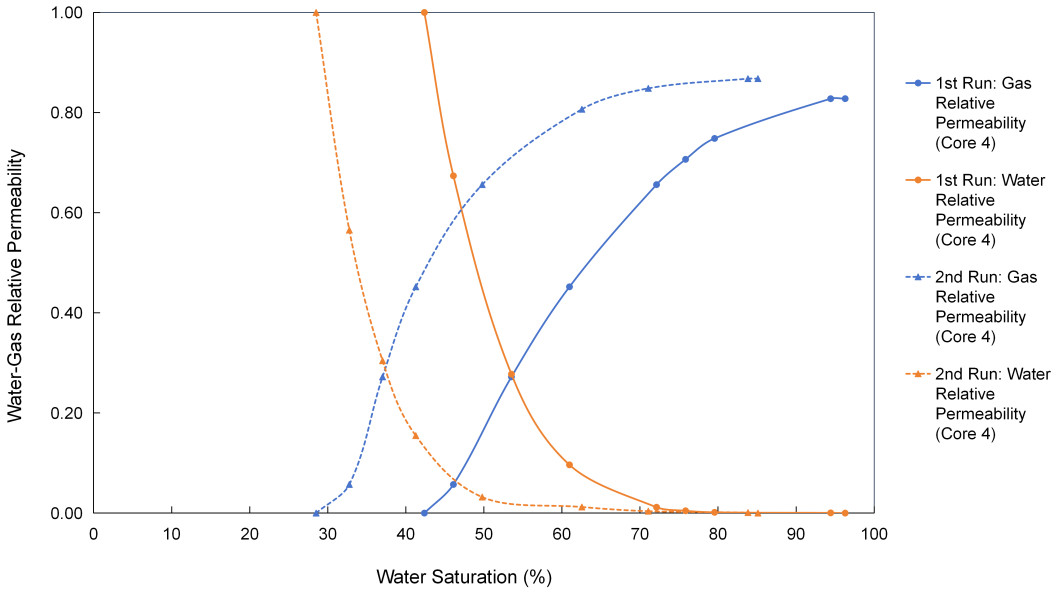

Fig. 5 Water–gas relative permeability curves (experimental group 4)

(Cores 3 and 4) are more sensitive to multi-cycle injection–production. They exhibit a larger increase in residual gas saturation and greater dispersion in relative permeability curves. This is primarily because the pore throats in low-permeability reservoirs are small and capillary forces dominate, making gas more easily snapped off and trapped. For such UGS facilities, it is recommended to adopt a more moderate pressure fluctuation range in operation strategies, or consider measures such as surfactant injection to improve gas–water interfacial tension, thereby alleviating gas phase trapping and enhancing turnover efficiency.

5 Conclusions

(1) Significant relative permeability hysteresis: during multi-cycle injection–production in depleted-gas-reservoir UGS, gas–water relative permeability exhibits pronounced cyclic hysteresis characteristics. With increasing injection–production cycles, the gas relative permeability curve shifts downward overall and the flow capacity declines; the change in water relative permeability is relatively small, but distinct variations in threshold pressure gradient are observed in low-permeability reservoirs.

(2) Cumulative effect of residual gas: Multi-cycle operation

leads to a significant accumulation of residual gas saturation, with an average increase of 12%–15%, and the increase is even more drastic in low-permeability reservoirs. This is the main reason for the decline in gas flow capacity and the attenuation of effective storage capacity.

(3) Complexity of pressure boosting and capacity expansion: Raising the operating pressure (from 40 MPa to 45 MPa) can lower irreducible water saturation and increase the total gas-filled pore volume; however, it simultaneously exacerbates gas phase trapping, causing a further increase in residual gas saturation. The pressure boosting and capacity expansion scheme must comprehensively balance the contradiction between the increase in total storage capacity and the decrease in effectively recoverable geological reserves.

(4) Engineering recommendations: In the full life-cycle management of UGS, a storage capacity evaluation model based on dynamic relative permeability should be established, and the relative permeability parameters should be updated regularly. For low-permeability UGS and aging UGS undergoing pressure-boosting operations, particular attention should be paid to monitoring the evolution of residual gas saturation and optimizing the injection–production pressure differential system, so as to delay the decline of flow capacity and maximize the peak-shaving benefits of UGS.

Acknowledgements

This work is financially supported by National Science and Technology Major Projects of China (Grant No.2024ZD1004300 and No.2025ZD1406404), National Natural Science Foundation of China (Grant No. 52474086), Hubei Provincial Natural Science Foundation of China (Grant No. 2025AFA092) and Sichuan Province International Science and Technology Innovation Cooperation Program.

Conflict of interest

The authors declare no competing interest.

References

Amri A, Saâdi Z, Ababou R. 2024. Modeling Two-Phase Flow with Hysteresis: Comparative Study of Hysteresis Models and Application. *Rock Mechanics and Rock Engineering*, **57**(6): 4333–4354. doi:10.1007/s00603-023-03501-1.

Bian CS, Wang ZC, Xu ZH, et al. 2014. Control of tectonic subsidence gradient on the development of sedimentary systems in basins. *China Petroleum Exploration*, **19**(3): 33–42. doi:10.3969/j.issn.1672-7703.2014.03.004.

Carlson FM. 1981. Simulation of relative permeability hysteresis to the nonwetting phase. *SPE Annual Technical Conference and Exhibition*, SPE-10157-MS.

Deng P, Chen ZX, Peng XL, et al. 2023. Optimized lower pressure limit for condensate underground gas storage using a dynamic pseudo-component model. *Energy*, **285**(3):129505. doi:10.1016/j.energy.2023.129505.

Deng GR, Zhou JP, Tian SF, et al. 2023. Pore structure changes and its stress-sensitive behavior in sandstone under cyclic stress: Implication for underground gas storage. *Gas Science and Engineering*, **119**:205130. doi:10.1016/j.jgsce.2023.205130.

Du J, Zhu GH, Wu LF, et al. 2021. 'Multi–formation quasi–continuous' accumulation model of tight gas in the Linxing area and exploration practice of a large gas field. *Natural Gas Industry*, **41**(3): 52–61. doi:10.3787/j.issn.1000-0976.2021.03.007.

Du J, Zhu GH, Li Y, et al. 2022. Challenges and technical countermeasures for exploration and development of tight sandstone gas reservoirs in the margin of the Ordos Basin: A case study of the Linxing–Shenfu gas field. *Natural Gas Industry*, **42**(1): 89–98. doi:10.3787/j.issn.1000-0976.2022.01.011.

Fatemi SM. 2015. Multiphase flow and hysteresis phenomena in oil recovery by water alternating gas (WAG) injection. *Heriot-Watt University*.

Foroudi S, Gharavi A, Fatemi M. 2022. Assessment of two-phase relative permeability hysteresis models for oil/water, gas/water and gas/oil systems in mixed-wet porous media. *Fuel*, **309**: 122150. doi:10.1016/j.fuel.2021.122150.

Gao GL, Liu W, Zhu SJ, et al. 2022. Discussion on the reconstruction of medium/low-permeability gas reservoirs based on seepage characteristics. *Processes*, **10**(4): 756. doi:10.3390/pr10040756.

Gao JD, Kong DB, Peng YF, et al. 2023. Pore-scale mechanisms and hysteresis effect during multi-cycle injection and production process in underground hydrogen storage reservoir. *Energy*, **283**: 129007. doi:10.1016/j.energy.2023.129007.

Gao YB, Chu HY, Ren ZQ, et al. 2025. Impact of relative permeability hysteresis on pressure transient behavior and storage capacity in underground gas storage with well interference. *Energy*, **333**: 137402. doi:10.1016/j.energy.2025.137402.

He FQ, Wang FB, Zhang W, et al. 2020. Exploration thought transformation and major breakthrough in the natural gas domain in the northern margin of the Ordos Basin. *China Petroleum Exploration*, **25**(6): 34–45. doi:10.3969/j.issn.1672-7703.2020.06.004.

He YT, Tian SC, Song XZ, et al. 2026. Experimental Investigation of Caprock Wettability and Helium-water Interfacial Tension: Implications for Structural Gas Geostorage Capacity Estimation. *GeoStorage*, **2**(2): 98–105. doi:10.46690/gs.2026.02.01.

Hu CY, Li C, Yang ZB, et al. 2024. Quantitative evaluation of maximum operating pressure and storage capacity for gas-top sandstone reservoir-type gas storage. *Journal of Geomechanics*, **30**(3):419–426. doi:10.12090/j.issn.1006-6616.2023075.

Huang ZL, Chen DS, Ren JF, et al. 2012. Dolomite reservoir and trap accumulation characteristics of the Middle Ordovician in the Ordos Basin. *Acta Petrolei Sinica*, **33**(S2): 118–124.

Jello J, Khan M, Malkewicz N, et al. 2022. Advanced geothermal energy storage systems by repurposing existing oil and gas wells: A full-scale experimental and numerical investigation. *Renewable Energy*, **199**: 852–865. doi:10.1016/j.renene.2022.07.145.

Johnson EF, Bossler DP, Bossler VON. 1959. Calculation of relative permeability from displacement experiments. *Transactions of the AIME*, **216**(01): 370–372. doi:10.2118/1023-G.

Jones SC, Roszelle WO. 1978. Graphical techniques for determining relative permeability from displacement experiments. *Journal of Petroleum Technology*, **30**(05): 807–817.

doi:10.2118/6045-PA.

Killough JE. 1976. Reservoir simulation with history-dependent saturation functions. *Society of Petroleum Engineers Journal*, **16**(01): 37–48.

Land CS. 1968. Calculation of imbibition relative permeability for two-and three-phase flow from rock properties. *Society of Petroleum Engineers Journal*, **8**(02): 149–156.

Mehdi H, Koederitz LF, Harvey AH. 1986. Relative permeability of petroleum reservoirs. *Boca Raton: CRC Press*. doi:10.1201/9781351076326.

Mi LJ, Zhu GH. 2021. Accumulation geological characteristics and exploration breakthrough of the Linxing–Shenfu tight gas field in the northeastern margin of the Ordos Basin. *China Petroleum Exploration*, **26**(3): 45–56. doi:10.3969/j.issn.1672-7703.2021.03.005.

Mi ZX, Wang FG, Shi N, et al. 2018. Experimental study on effect of multi-stage stress variations on permeability and pore structure of sandstone. *Chinese Journal of Geotechnical Engineering*, **40**(5): 864–871. doi:10.11779/CJGE201805011.

Song Y, Song ZJ, Chen ZX, et al. 2024. Fluid phase behavior in multi-scale shale reservoirs with nano-confinement effect. *Energy*, **289**: 130027. doi:10.1016/j.energy.2023.130027.

Spiteri E J, Juanes R, Blunt M J, et al. 2008. A new model of trapping and relative permeability hysteresis for all wettability characteristics. *SPE Journal*, **13**(03): 277–288. doi:10.2118/96448-PA.

Thabit A, Stephen K D. 2025. Relative Permeability from Unsteady-State Displacement Experiments: A Novel Analytical Estimation Technique. *SPE Annual Caspian Technical Conference*, D021S009R005.

Wang HM, Tian JL, Lin JX, et al. 2025. NMR investigation on pore-scale stress sensitivity during pore fluid pumping cycles: Implication for geological fluid storage. *International Journal of Hydrogen Energy*, **120**: 1–12. doi:10.1016/j.ijhydene.2025.03.269.

Wang Q, Zhang M, Zhou F, et al. 2024. Experiment and prediction of enhanced gas storage capacity in depleted gas reservoirs for clean energy applications. *Renewable Energy*, **237**: 121894. doi:10.1016/j.renene.2024.121894.

Wang Q, Zhou FJ, Su H, et al. 2024. Experimental evaluations of nano high-viscosity friction reducers to improve acid fracturing efficiency in low-permeability carbonate reservoirs. *Chemical Engineering Journal*, **483**: 149358. doi:10.1016/j.cej.2024.149358.

Wei H, Zhong Z, Cheng JM, et al. 2026. The underground gas storage capacity evaluation-A case study from depleted oil reservoirs to underground gas storage. *Fuel*, **406**: 137079. doi:10.1016/j.fuel.2025.137079.

Yang SY, Hu SL, Qi ZL, et al. 2024. Experiment and prediction for dynamic storage capacity of underground gas storage rebuilt from hydrocarbon reservoir. *Renewable Energy*, **222**: 119908. doi:10.1016/j.renene.2023.119908.

Yang Z, Li C, Hu C, et al. 2023. Scheme Design of Rebuilding Gas-Cap Sandstone Reservoirs into Underground Gas Storage. *International Field Exploration and Development Conference*, 924–941. doi:10.1007/978-981-97-0268-8_73.